# Myomegalin regulates Hedgehog pathway by controlling PDE4D at the centrosome

Hualing Peng[1*], Jingyi Zhang[1*], Amanda Ya[1,2], Winston Ma[1], Xuecai Ge[1**]

[1]Department of Molecular and Cell Biology, University of California, Merced, Merced, CA 95340
[2]Current address: Molecular and Cell Biology Program at Dartmouth College, Hanover, NH 03755

* These authors contribute equally to this work
** Correspondence: xge2@ucmerced.edu

## Abstract

Mutations in the Hedgehog (Hh) signaling are implicated in birth defects and cancers, including medulloblastoma, one of the most malignant pediatric brain tumors. Current Hh inhibitors face the challenge of drug resistance and tumor relapse, urging new insights in the Hh pathway regulation. Our previous study revealed how PDE4D controls global levels of cAMP in the cytoplasm to positively regulate Hh signaling; in the present study we found that a specific isoform PDE4D3 is tethered to the centrosome by myomegalin, a centrosome/Golgi associated protein. Myomegalin loss dislocates PDE4D3 from the centrosome, leading to local PKA over-activation and inhibition of the Hh signaling, leaving other PKA-related pathways unaffected. Myomegalin loss suppresses the proliferation of granule neuron precursors, and blocks the growth of medulloblastoma in mouse model. Our findings specify a new regulatory mechanism of the Hh pathway, and highlight an exciting therapeutic avenue for Hh-related cancers with reduced side effects.

## Introduction

The Hedgehog (Hh) pathway is widely implicated in birth defects and human tumors[1]. The Hh ligand, Sonic Hedgehog (Shh), acts as a mitogen to stimulate the proliferation of granule neuron precursors in the developing cerebellum[2–4]. Over-activating mutations in Hh pathways leads to medulloblastoma, one of the most malignant pediatric brain tumors[5]. Hh signal transduction involves a series of protein transport into and out of the primary cilium, and eventually converges on the regulation of Gli transcription factors[6]. Without the ligand Sonic Hedgehog (Shh), the receptor Patched (Ptch) resides in the cilium, and prevents the cilium translocation and activation of Smoothened (Smo). Upon Shh stimulation, Ptch exits cilium; Smo enters cilium. The signaling cascade ultimately activates the transcription activator Gli2, and eliminates the transcription suppressor Gli3R[7]. Gli3R is a proteolytic product from Gli3[8]. Activated Hh signaling turns on the production of Gli1, which amplifies the Hh signaling, forming a positive feedback loop.

PKA plays a central role in Gli regulations. PKA phosphorylates Gli3; the phosphorylation sites are recognized by β-TrCP/SCF ubiquitin system that cleaves Gli3FL into Gli3R[8]. Within the cell, PKA concentrates at the centrosome (cilium base) where it controls the cilium translocation and the subsequent activation of Gli2[9]. Genetic removal of PKA leads to full activation of Hh pathway in the developing neural tube[9–11], further substantiating the strong inhibitory effect of PKA on Hh signaling. Conversely, pharmacological activation of PKA inhibits Hh signaling and suppresses Hh-related tumor growth[12,13]. However, PKA is widely involved in many signaling and metabolic pathways; ubiquitous activation of PKA inevitably impacts all pathways. It remains a challenge for the field to selectively control PKA activity in the Hh pathway while leaving other pathways unaffected.

PKA activity relies on the concentration of cAMP, which is precisely balanced by adenylyl cyclase that produces cAMP, and phosphodiesterase (PDE) that degrades cAMP. In our previous studies, we found that PDE4D, recruited to the cytoplasmic membrane by sema3-Neuropilin signaling, governs cAMP levels in the entire cell to regulate Hh signaling[14,15]. Our results were corroborated by Williams et al. who independently discovered PDE4D as a positive regulator of the Hh pathway in a chemical genetic screen in zebrafish[16]. Both studies demonstrated that globally inhibiting PDE4D activity in the entire cell with small chemical inhibitors suppressed the Hh pathway. Nevertheless, an established view in the field of phosphodiesterase suggests that PDE4D activity in the cell is compartmentalized; different isoforms of PDE4D are targeted to discrete subcellular sites where they modulate local cAMP levels that are essential for particular cellular events[17–19]. It is know that PKA at the centrosome directly regulates Hh transduction[9,20]; increasing PKA levels at the centrosome is sufficient to suppress the Hh signaling[20]. Therefore, strategies that can locally modulate cAMP levels at the centrosome might be effective to selectively affect Hh pathway. In the current study, we found that PDE4D3, tethered to the centrosome by PDE4DIP/Myomegalin (Mmg)[21], specifically regulates the Hh pathway. Silencing Mmg expression dislocates PDE4D from the centrosome, leading to local PKA hyperactivity. This dampens Hh activity while sparing other PKA -related cellular events, and suppresses Hh-related tumor growth in mouse model. Our study, for the first time, demonstrates an effective mechanism to control centrosomal PKA activity in order to selectively inhibit the Hh pathway. It highlights an exciting avenue to treat Hh-related cancers with reduced side effects.

## Results

### Myomegalin (Mmg) interacts with PDE4D3 at the centrosome

To identify an effective approach of selectively modulating cAMP levels at the centrosome, we did a literature search on the subcellular localization of all cAMP-specific phosphodiesterases. We found that one PDE4D isoform, PDE4D3 was reported to interact with Mmg, a protein associated with the centrosome/Golgi[21]. But it remains unclear whether PDE4D3 localizes to the centrosome and whether it is involved in the regulation of the Hh signaling. To answer these questions, we first validated the Mmg-PDE4D3 interaction. Mmg is a large protein of 270KD, and the full-length protein is not effectively expressed in cells. But in the previous study the C-terminus of Mmg was identified to mediate its interaction with PDE4D3[21] (Fig. 1A). We thus fused this domain (Mmg-C) with Flag and expressed it together with HA-PDE4D3 in the cell. We then performed co-immunoprecipitation assay with Flag- and HA- conjugated magnetic beads, and found that two proteins co-immunoprecipitated each other (Fig. 1B). This result suggests that PDE4D3 and Mmg interact with each other.

We then validated the localization of Mmg to the centrosome/Golgi region with immunofluorescence staining[22]. Mmg immunofluorescence significantly overlaps with pericentrin, a marker of the centrioles and pericentriolar material (Fig. 1C). The non-centrosomal Mmg signal may represent its localization to Golgi. Intriguingly, HA-PDE4D3, when expressed in NIH3T3 cells, concentrates at the centrosome, although its diffusive distribution to the cytosol is also noticeable (Fig. 1D). Finally, when expressed together, HA-PDE4D3 and Flag-Mmg overlap significantly at the centrosome/Golgi area (Fig. 1E). As PDE4D3 does not contain any characteristic centrosomal localization sequence, it is very likely that PDE4D3 is anchored to the centrosome by Mmg. Therefore, our results suggest that Mmg and PDE4D3 interact with each other at the centrosome.

### Mmg loss impairs Hh signal transduction and dislocates PDE4D3 from the centrosome

Next, we tested whether eliminating PDE4D3 from the centrosome impacts the Hh pathway. We silenced Mmg expression with shRNA in NIH3T3 cells, a cell line that contains all components of the Hh pathways and is commonly used to study Hh signaling transduction. Two of the five tested shRNAs significantly reduced the transcript and the protein levels of Mmg (Fig.

2-supplement 1A-B). We then treated cells with SAG, a small molecule agonist of the Hh pathway, and assessed the Hh Hh pathway activation with qPCR measuring the transcript level of Hh target gene Gli1. Mmg shRNA significantly reduced SAG-induced Gli1 expression, indicating that Hh signal transduction was impaired (Fig. 2-supplement 1C).

To confirm our shRNA data, we employed CRISPR to knockout Mmg in MEF. We choose MEF because it transduces Hh signaling but has lower ploidy level than NIH3T3 cells. We used two gRNAs targeting the 1st exon of Mmg (Fig. 2-Supplement 2A), and transfected the plasmid containing the two gRNAs and Cas9 into MEF cells, together with EGFP. Single cell clones were isolated via flow cytometry and expanded (Fig. 2A). We obtained two cell clones (#7, #10) of Mmg knockout (Fig. 2B-C). Both clones appear normal in cell morphology and cell proliferate (data not shown), with undetectable Mmg transcript levels. Interestingly, among the 4 alternative splicing isoforms of mouse Mmg (https://www.ncbi.nlm.nih.gov/gene/83679), CRISPR abolished the expression of the longer isoforms (~270KD) and spared the shorter isoform (~130KD) (Fig. 2C), presumably because the shorter isoform uses an alternative transcription starting point. The shorter isoform, however, does not interact with PDE4D3 as it lacks the C-terminus. To identify the INDEL mutations induced by CRISPR, We cloned exon 1 and its flanking region with PCR in Mmg CRISPR clones, and sequenced individual PCR products (Fig.2-supplement 2B-1C). The sequencing results show that 3 type of mutations were generated in each clone, resulting in frameshift that eventually leads to nonsense-mediated mRNA decay.

To determine the Hh signaling in Mmg knockout clones, we stimulated cells with SAG, and detected Gli1 expression with qPCR and western blot. SAG-induced Gli1 expression was dramatically reduced at the transcript and protein levels in both clones (Fig. 2D-E). These results suggest a blockage of Hh transduction after Mmg loss.

Next we determined the impact of Mmg loss on PDE4D3 localization. Due to the high similarity between PDE4D isoforms, the antibody specific to PDE4D3 is unavailable. Therefore, we expressed EGFP-PDE4D3 in Mmg knockout clones, and focused on cells with only low expression levels. PDE4D3 concentrates at the centrosome in wild type MEF (Fig. 2F). However, in Mmg knockout clones, PDE4D3 only exhibits diffusive localization to the cytoplasm, and the intensity at the centrosome is significantly reduced (Fig. 2F-G). Apparently, Mmg loss of function dislocates PDE4D3 from the centrosome.

In summary, our data suggests that loss of Mmg markedly suppresses Hh signal transduction, and dislocates PDE4D3 from the centrosome.

**Mmg loss over-activates PKA at the centrosome**

Dislocation of PDE4D3 from the centrosome may increase local cAMP levels, which eventually leads to PKA over-activation. To quantify the local active PKA levels, we stained cells with an antibody that recognizes active PKA (phosphoPKA T197). This antibody has been used to evaluate PKA activity in previous studies of our group and others[9,15,20]. We highlighted the centrosome and pericentriolar area with pericentrin staining, and measured the phosphoPKA levels in this area in ImageJ. As expected, the centrosomal active PKA levels are much higher in Mmg knock out cells compared to that in wild type MEF (Fig. 3A-B). Further, expressing exogenous Mmg in Knockout clones restored active PKA levels to normal (Fig. 3B). This change of PKA activity, however, is limited locally to the centrosome, since the overall phosphoPKA levels remain the same in Mmg Knockout clones (Fig. 3C).

We then assessed the impact of PKA on other cAMP-related cellular processes. One important PKA substrate that is broadly involved in many biological events is CREB (cAMP-response element binding protein). As a ubiquitous transcription factor, CREB controls the transcription of a wide range of target genes[23]. CREB stimulates target gene transcription after phosphorylation by PKA at S133. We found that the phosphoCREB levels remain unchanged in Mmg knockout cells (Fig. 3C), indicating that the CREB-mediated cellular events are not affected by Mmg loss.

The transcription factor Gli2 and Gli3 are PKA substrates in the Hh pathway. After PKA phosphorylation, Gli3 is proteolytically processed into Gli3R, a transcription repressor[6,8] (Fig. 3D). Upon Hh signaling activation, the Gli3 processing ceases and Gli3R levels markedly reduce[24,25]. We examined Gli3 processing by western blot. In wild type cells, SAG treatment significantly reduced Gli3R levels in cell lysates. In contrast, in Mmg CRISPR clones, the Gli3R levels remain the same after SAG treatment (Fig. 3E). It is likely that without Mmg, the hyperactive PKA at the centrosome continues to phosphorylate Gli3 to promote Gli3R production even after SAG treatment. PKA affects the proteolysis of Gli2 only very slightly but more dramatically controls its accumulation at cilia tips, a step required for Gli2 activation[9,24,25]. We then quantified Gli2 enrichment at the cilium tips after SAG treatment. The Gli2 intensity at the cilium tips in Mmg Knockout clones was significantly lower, compared to that in wild type cells (Fig. 3F-G). When exogenous Mmg was expressed in Knockout clones, it restored the levels of Gli2 at the cilium tips (Fig. 3F-G). As a conclusion, Mmg loss overactivates PKA at the centrosome, which blocks Gli2 transport to the cilium tips and keeps Gli3R levels high, leading to inhibition of the Hh signaling.

In summary, our data suggest a model of how Mmg and PDE4D3 at the centrosome control local PKA activity to regulate the Hh pathway (Fig. 3-supplement 1). Under normal conditions, Shh stimulation eventually leads to decreased cAMP levels, thus PKA inactivation, at the centrosome/cilium base, as combined effects of reduced cAMP production and cAMP degradation by local PDE4D3. The inactive PKA at the centrosome allows Gli2 to be translocated and activated in the cilium tips, and stops Gli3R production, leading to Hh pathway activation. When PDE4D3 is dislocated from the centrosome, local cAMP, diffused from other subcellular sites, is not effectively degraded and the PKA activity remains high. This suppresses Gli2 activation and keeps Gli3R levels high, which blocks the activation of Hh signaling.

**Mmg loss blocks cell proliferation in primary cultured granule neuron precursors (GNPs)**

In the developing cerebellum, Shh is the mitogen that stimulates GNP proliferation[2–4]. Overactive Hh signaling leads to GNP over proliferation that eventually results as medulloblastoma (MB), one of the most malignant pediatric brain tumor[26]. Both PDE4D3 and Mmg (www.informatics.jax.org/assay/MGI:5421053) are highly expressed in the developing cerebellum[27]; it is likely that the mechanism of Mmg-PDE4D3 regulation on Hh pathway applies to the control of GNP proliferation. To test this hypothesis, we cultured GNPs from p7 mouse neonates in dishes, and infected GNPs with lentiviral particles expressing shRNA against Mmg (Fig. 4A). GNP proliferation was induced by SAG. After 3 days of primary culture, GNP proliferation was assessed by BrdU incorporation assay. As expected, Mmg shRNA significantly reduced Mmg transcript levels, and reduced the rate of BrdU incorporation after pulse labeling (Fig. 4B-D). Hence, our results suggest that the same mechanism of Hh signaling regulation by Mmg-PDE4D3 controls GNP proliferation in the developing cerebellum.

**Mmg loss reduced the growth rate of medulloblastoma in mouse model**

Next, we assess the effect of Mmg loss on the Hh-related tumor growth in the mouse model of MB subcutaneous xenograft used in our previous studies[15]. We employed MB56, MB tumor cells directly taken from Ptch$^{+/-}$ mouse, the first and well-established MB mouse model[5,28]. We infected MB56 with lentiviral particles that express Mmg (shRNA #99) or control shRNA (Fig. 2-Supplement 1). 2 days after infection, tumor cells were injected subcutaneously in the hind flank of nude mice. 6 days after injection, tumors size was measured daily for two weeks (Fig. 5A). We found that Mmg loss significantly slowed tumor growth starting from day 4 of measurement (Fig. 5B). At the end of the experiment, we evaluated Gli1 levels in randomly sampled tumors and found that Mmg loss significantly reduced Hh signal activity (Fig. 5C). Thus, knockdown of Mmg suppressed the growth of Hh-related tumors.

## Discussion

Genetic removal of PKA leads to full activation of the Hh pathway in the developing neural tube[9,10], suggesting PKA as a strong inhibitor of the Hh signaling. However, as a multifaceted enzyme, PKA is widely involved in many signaling and metabolic pathways. It is a challenge to specifically control PKA activities in the Hh signaling while keeping other pathways unaffected. Our previous study pointed PDE4D as a potential target to inhibit Hh signaling[15]. Our current study is based on an established view in the field of PDE4D-cAMP that distinct PDE4D isoforms are localized to discrete subcellular compartments, where they locally tailor cAMP levels for specific cellular events[18]. For the first time, we provide evidence that dislocating PDE4D3 from the centrosome overactivates PKA locally at the centrosome to inhibits the Hh pathway, while sparing other PKA-related cellular events. It shed light on a new regulatory mechanism of Hh pathway regulation, and highlighted a potential therapeutic avenue to treat Hh-related tumors with reduced side effects.

Cells have evolved two mechanisms to accurately govern local levels of cAMP and PKA activity: 1) controlling its production by adenylyl cyclase, and 2) managing its degradation by cAMP specific PDEs. Previous studies on Smo and GPR161 elegantly demonstrated how cAMP production is controlled by Hh signaling. Upon Hh activation, Smo in the cilium activates Gαi subunit, which inhibits adenylyl cyclase to stop cAMP production[29]. GPR161 resides at the cilium when Hh pathway is off, where it activates the Gαs subunit and keeps the local cAMP levels high[30]. Upon Hh activation, GPR161 exits the cilium and stops cAMP production. However, cAMP is highly diffusible; ceasing cAMP production at the cilium may not be effective enough to shut down PKA activity at the centrosome, since cAMP will diffuse from neighbor subcellular sites. Therefore a 2$^{nd}$ mechanism comes in place to eliminate cAMP by PDE4D. This insight of cAMP modulation in Hh signaling was only recently demonstrated by our previous study on sema3-Neuropilin-PDE4D pathway[14,31], and by Williams et al. who independently discovered PDE4D as a positively regulator of the Hh signaling[16]. Our currently study identified an anchor mechanism of PDE4D3 to the centrosome by Mmg, and pinpointed the specific cellular machinery that controls cAMP levels in the Hh pathway.

PDE4D is a large protein family comprising more than 12 alternative splicing isoforms in mammalian cells[32]. PDE4D3 was originally identified to bind to Mmg by Verde et al (2001). Besides PDE4D3, other isoforms could be tethered to the centrosome as well, and Mmg loss might dislocate all these isoforms from the centrosome. If so, the strong Hh inhibition after Mmg loss could be combined effects of dislocating all these isoforms from the centrosome.

Finally, our study highlighted an effective method for Hh-related cancer treatment. Current Hh inhibitors target Smo, and these inhibitors are facing challenges of drug resistance and tumor relapse[33]. Since the Mmg-PDE4D-PKA axis acts directly at Gli transcription factors, downstream of Smo, targeting this axis will be effective for cancers that have developed resistance to Smo inhibitors. Further, it is known that the basal activity of PDE4D is high, and most PDE4D small molecular inhibitors act by blocking the catalytic domain of PDE4D[34]. These inhibitors unavoidably inhibit all PDE4D isoforms thereby being associated with severe side effects. However, our current study suggests that we may eliminate PDE4D activity specifically from the centrosome without blocking its catalytic domain. It pinpointed an effective therapeutic avenue to treat Hh-related cancers with reduced side effects.

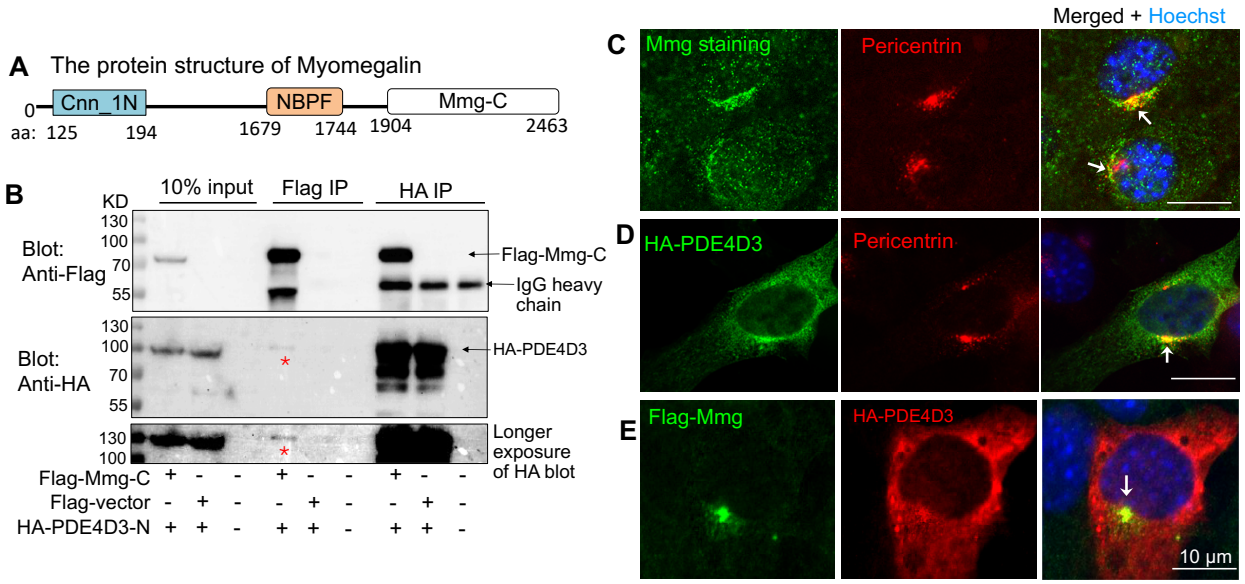


**Figure 1. PDE4D3 interacts with Mmg at the centrosome.**
(A) Protein structure of Mmg. Cnn_1N, Centrosomin N-terminal motif 1; NBPF (DUF1220), domain of Neuroblastoma breakpoint family; Mmg-C, the domain previously shown to interact with PDE4D3. (B) When overexpressed in HEK293T cells, HA-PDE4D3 and Flag-Mmg co-immunoprecipitated with each other, suggesting the interaction of the two proteins. (C) Representative images of Mmg immunofluorescent staining in NIH3T3 cells show that Mmg localizes to the centrosome and pericentriolar material (white arrows). Its non-centrosomal signal may represent Golgi body. (D) When overexpressed in NIH3T3 cells, HA-PDE4D3 diffusively distribute to the cytoplasm, and concentrates at the centrosome and pericentriolar material (white arrow). (E) Colocalization of Flag-Mmg and HA-PDE4D3 at the centrosome and pericentriolar material (white arrow).

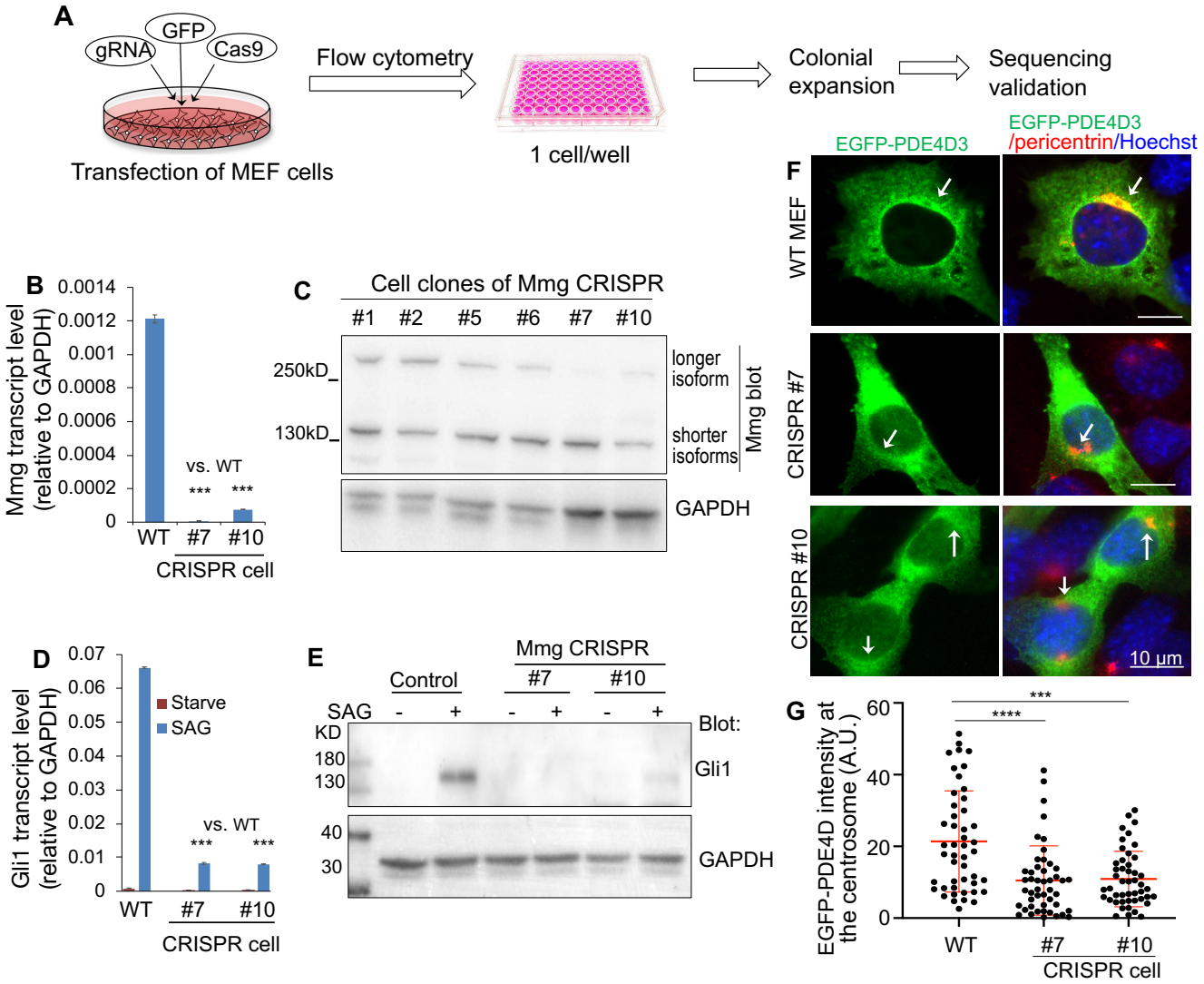


**Figure 2. Mmg knockout impairs Hh signal transduction and dislocates PDE4D from the centrosome.**

(A) Procedure of generating Mmg CRISPR cell clones. 30 cell clones were established, and were tested with qPCR for Mmg transcript levels, followed by western blot for Mmg protein levels. (B) In two of the Mmg CRISPR cell clones, the transcript of Mmg was hardly detectable by qPCR. (C) Western blot shows that in cell clone #7 and #10, the CRISPR abolished the expression of the longer isoforms of Mmg, but the shorter isoform remains unaffected. (D-E) Mmg CRISPR knockout clones were stimulated with SAG for 24hr, and Hh signaling activity was evaluated by Gli1 transcript levels and protein levels. The Hh activity was dramatically suppressed in Mmg knockout cells. (F) Representative images of EGFP-PDE4D3 expressed in wild type or Mmg knockout cell clones. PDE4D3 concentrates at the centrosome and pericentriolar material in wild type cells (white arrow); however, in CRISPR cell clones, it only exhibits diffusive distribution to the cytoplasm and lacks the significant overlap with pericentrin (white arrows). (G) Quantification of PDE4D intensity at the centrosome. All error bars represent SD; statistics in B and D: Student's t-Test. **p<0.01, ***p<0.001. Statistics in G: Kruskal–Wallis non-parametric One-Way ANOVA, followed by Dunn's multiple comparison. ***p<0.001, ****p<0.0001. A.U.: arbitrary unit.

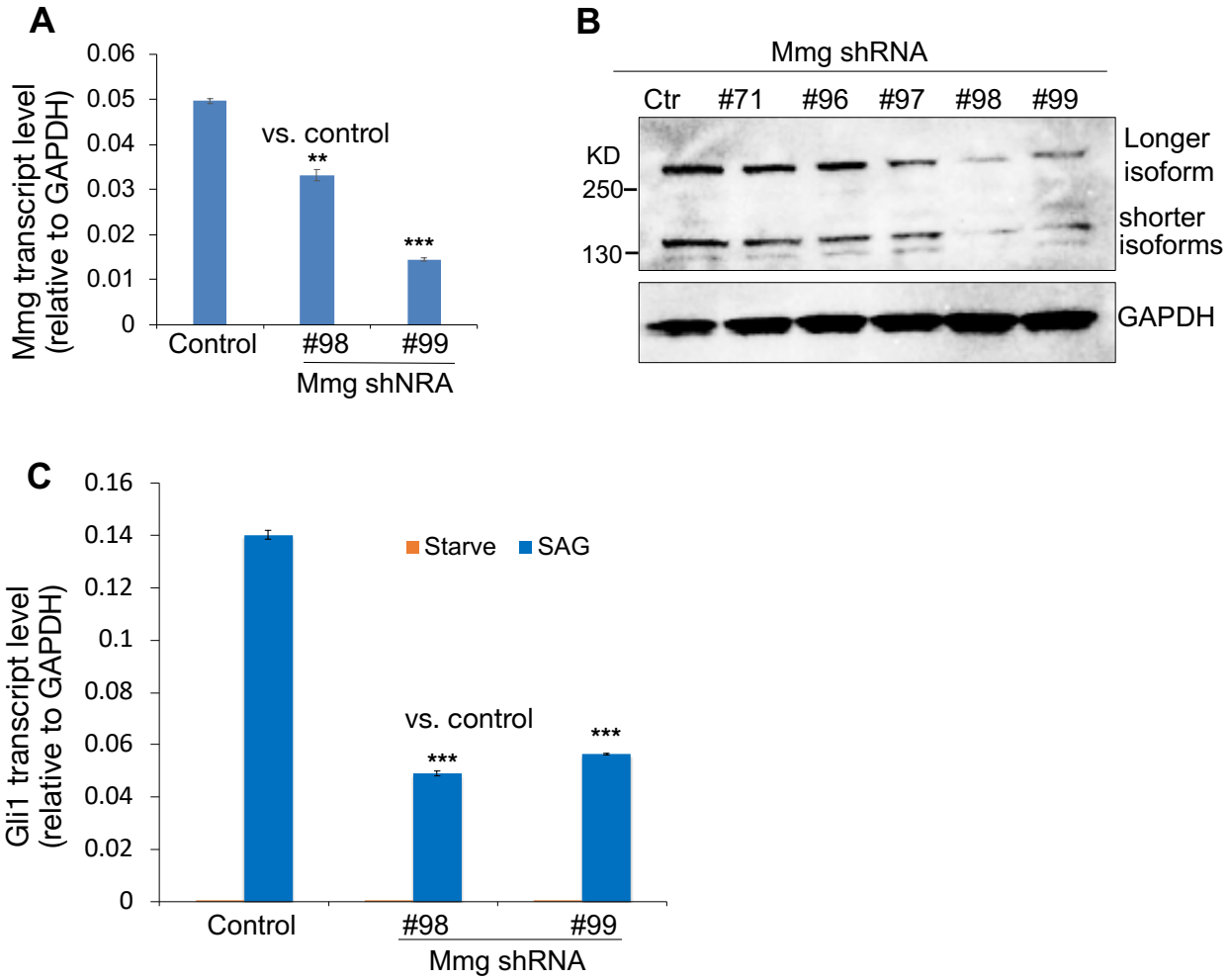


**Figure 2-supplement 1. Mmg knockdown impairs Hh signal transduction.**
(A) NIH3T3 cells were transfected with shRNA against myomegalin. 72hr after transfection, myomegalin transcript levels were assessed by qPCR. Two of the shRNAs significantly reduced Mmg transcription. (B) Western blot showing that among all the shRNAs tested, #98 and #99 decreased the Mmg protein expression levels. (C) 72hr after shRNA transfection, NIH3T3 cells were treated with SAG overnight. Hh signaling activity was evaluated by qPCR to detect the transcript levels of Gli1, a Hh pathway target gene. All error bars represent SD; statistics: Student's t-Test. **p<0.01, ***p<0.001.

## A. Genome targets of the two gRNAs

## B. Mutations in clone #7

*B1) 11bp insertion combined with 186bp deletion*

*B2) 4bp deletion*

*B3) 70bp insertion*

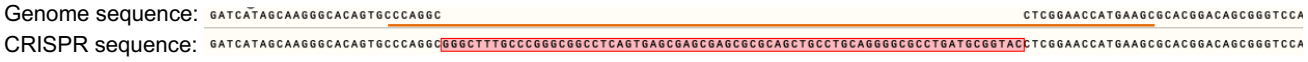


## C. Mutations in clone #10

C1) 2bp deletion

C2) 4bp deletion

C3) 1bp deletion

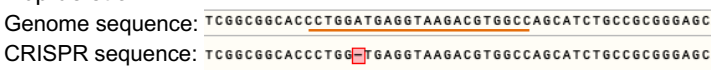


**Figure 2 Supplement 2. Design and results of Mmg CRISPR.**
(A) Design of Mmg CRISPR. Two guide RNAs were designed and both target exon 1 of mouse Mmg. Brown arrows underlie the sequence of gRNAs. (B-C) The gRNA targeting region in mouse genomic was cloned by genomic PCR, ligated into TOPO vector, and transfected into chemically competent cells. 20 bacterial colonies of each cell clones were randomly picked and sequenced. 3 type of mutations were found in cell line #7 (B) and #10 (C). No wild type sequences were identified in the 20 colonies, suggesting that all alleles of Mmg were mutated. Mutations lead to frame shift (B1, B2, C1, C2, C3), or alter the 5' UTR that prevents the initiation of translation, which eventually leads to nonsense-mediated decay (NMD) of the mutant mRNA.

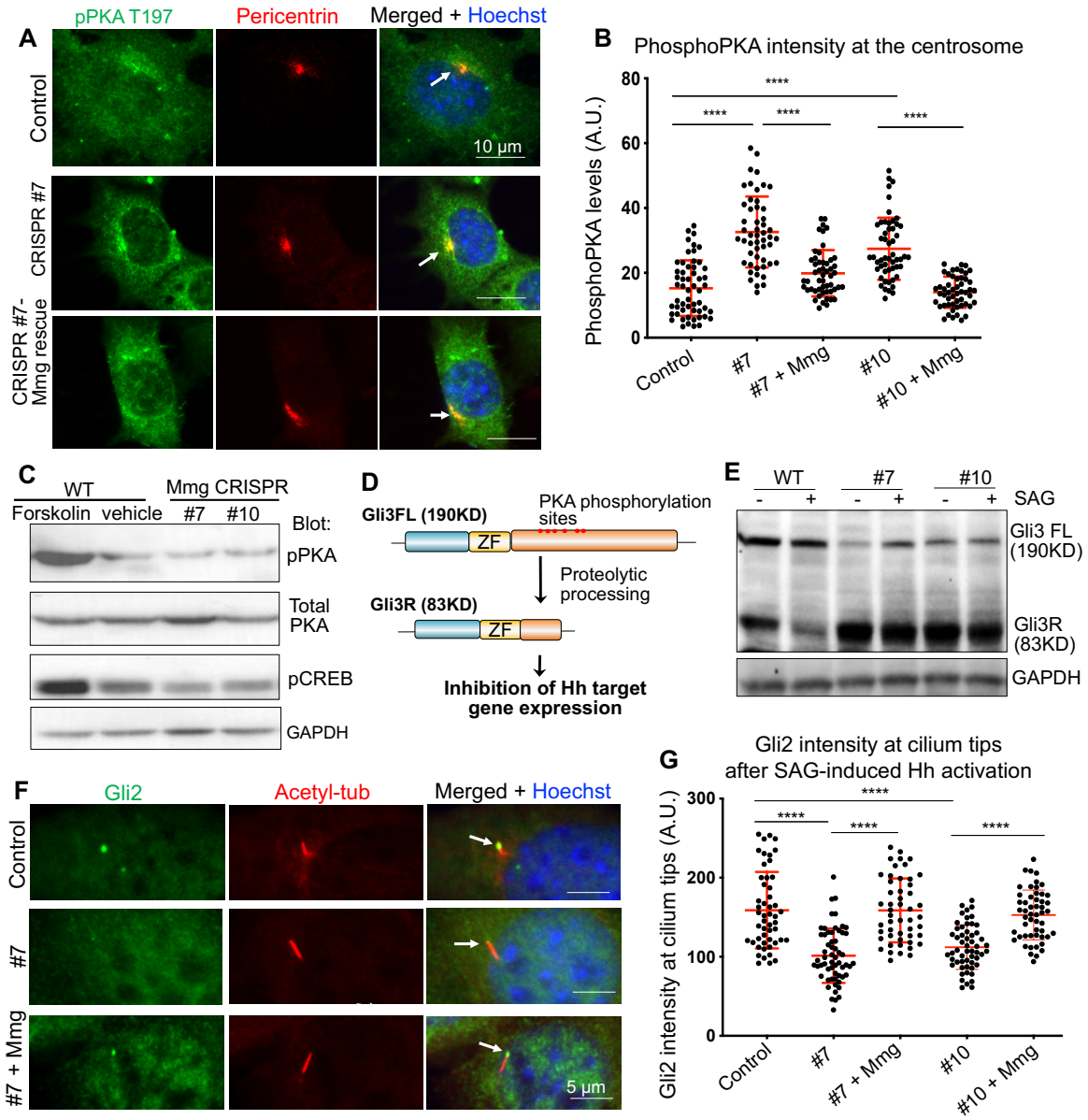


**Figure 3. Mmg loss over-activates PKA at the centrosome.**
(A) Representative images of active PKA immunostaining demonstrate that the active PKA levels at the centrosome increased in Mmg knockout cells (white arrows). (B) Quantification of active PKA levels at the centrosome. Expression of exogenous Mmg restored active PKA levels at the centrosome. (C) Western blot shows that the global levels of active PKA do not change in Mmg knockout cells. Forskolin induces cAMP production globally thereby serving as a positive control of PKA overactivation in the entire cell. The phosphorylation levels of CREB, a PKA substrate widely implicated in the transcription of many genes, does not change in Mmg knockout clones. (D) diagram showing the proteolytic processing of Gli3 after PKA phosphorylation. (E) 24hr SAG treatment reduced Gli3R levels in wild type cells, but not in Mmg knockout cell clones. (F) Representative images of Gli2 immunostaining after cells are stimulated with SAG. White arrows point to Gli2 at the cilium tips. (G) Quantification of Gli2 levels at the cilium tips. Mmg knockout reduced Gli2 levels at the cilium tips, while Mmg overexpression restored Gli2 intensity. (H) Diagram showing PED4D3 specifically controls PKA activities at the centrosome to regulate the Hh signaling transduction. Data in (B) and (G) are shown as mean ± SD. Statistics: Kruskal–Wallis non-parametric One-Way ANOVA, followed by Dunn's multiple comparison. ***p<0.001, ****p<0.0001. A.U.: arbitrary unit.

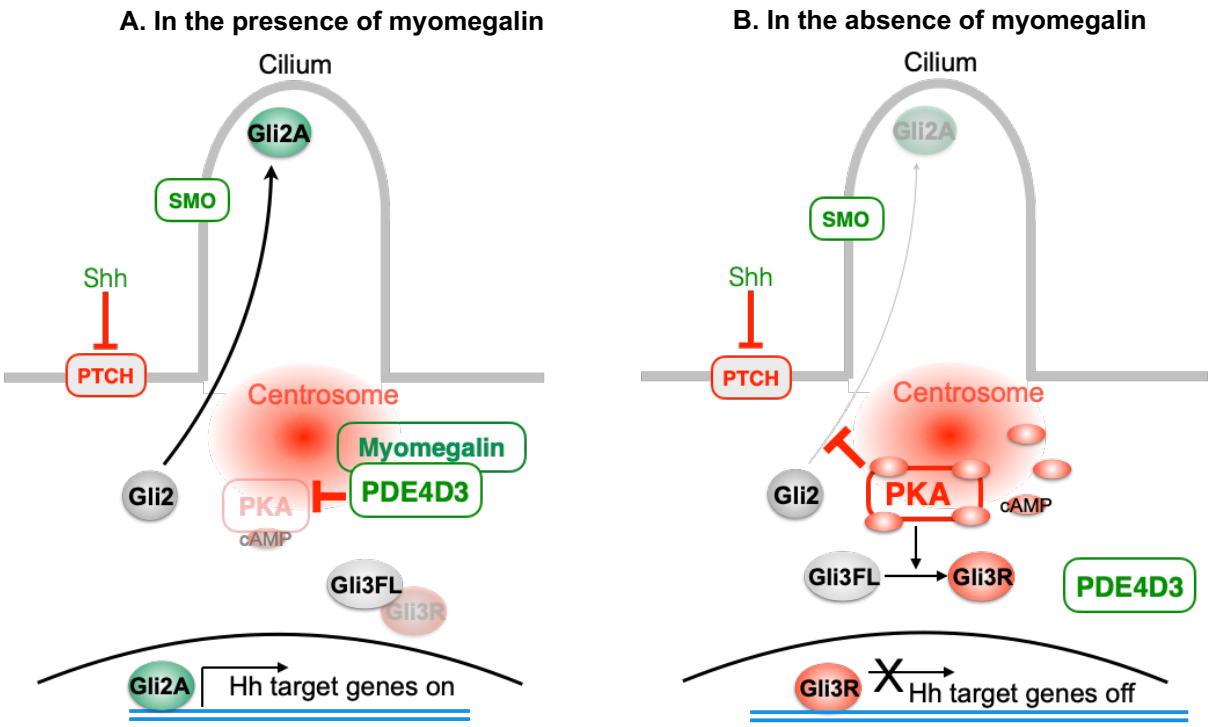


**Figure 3 - supplement 1. Diagram showing PED4D3 specifically controls PKA activities at the centrosome to regulate the Hh signaling transduction.**
(A) Under normal conditions, Shh binds to and inhibits the receptor PTCH, followed by SMO translocation and activation in the cilium. The signaling cascade eventually leads to reduced cAMP levels at the cilium base, as a combined effects of reduced cAMP production and cAMP degradation by local PDE4D3 at the centrosome. Subsequently PKA is inactivated, allowing Gli2 to be translocated and activated in the cilium tips. The inactive PKA also stops Gli3R production. As a result, active Gli2 (Gli2A) turns on transcription of Hh target genes. (B) Without myomegalin, PDE4D3 is dislocated from the centrosome and fails to degrade the local cAMP. Thus PKA levels remain high at the centrosome even after Shh stimulations. Hyperactive PKA suppresses Gli2 activation and promotes Gli3R production. As a result, the Hh target gene is off. Although cAMP production in the cilium ceases after Shh stimulation (Mukhopadhyay et al., 2013; Ogden et al., 2008), the local cAMP at the centrosome may be diffused from other subcellular sites.

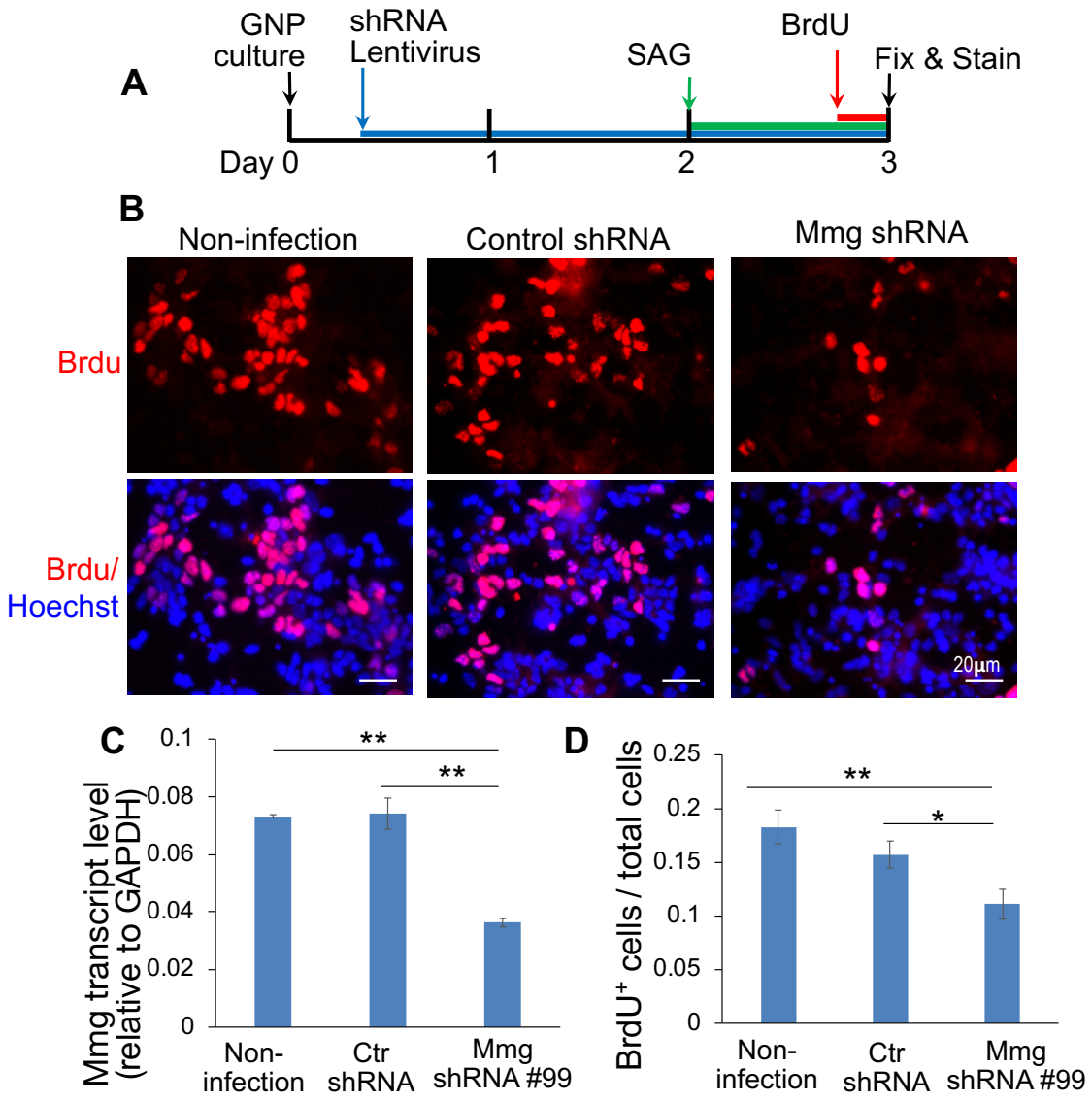


**Figure 4. Mmg knockdown blocked cell proliferation in primary cultured GNPs.**
(A) Schematic of BrdU incorporation assay in primary cultured GNPs. Lentivirus expressing shRNA against Mmg or control shRNA were added to the cell 5-6 hr after GNPs are plated in dishes. SAG was added to the culture 24 hr before cells were fixed. BrdU pulse labeling lasted for 4 hr right before cells were fixed. (B) Representative images of BrdU immunostaining in GNPs. (C) levels of Mmg transcript levels at the end of the experiments. (D) BrdU incorporation rate in GNPs. Data are presented as Mean ± SEM. Statistics: Student's t-Test. *$p<0.05$, **$p<0.01$.

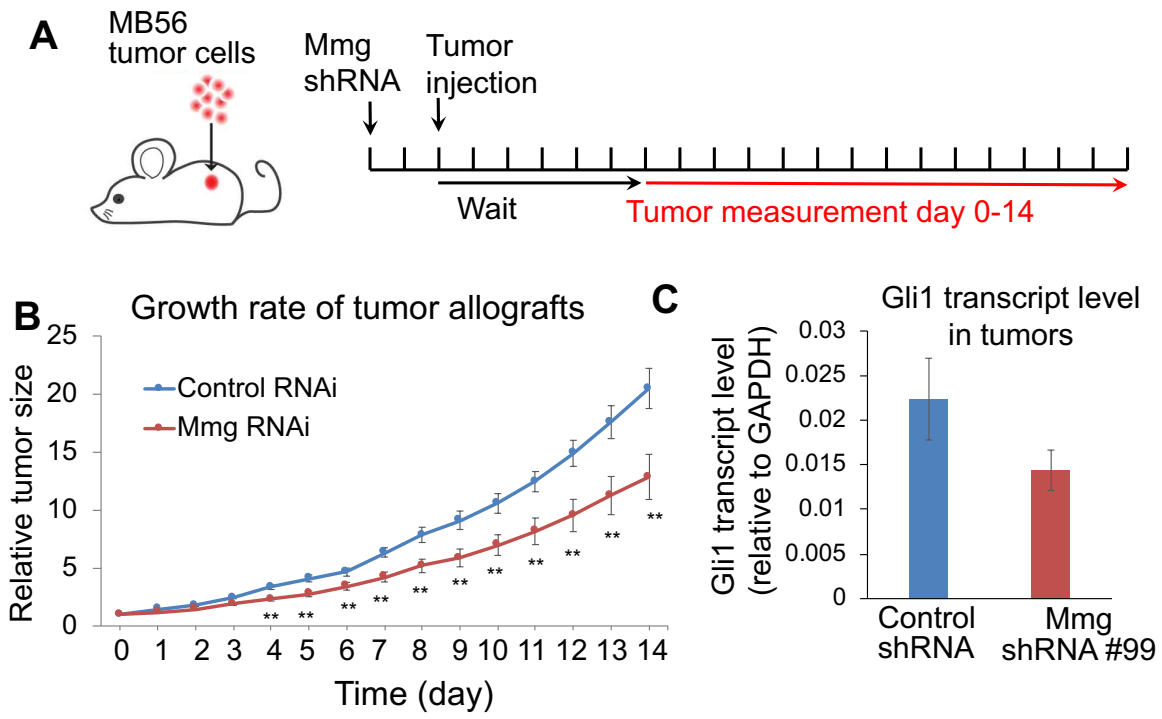


**Figure 5. Mmg knockdown reduced the growth rate of medulloblastoma in mouse model.** (A) Schematic diagram of the MB56 tumor allograft experiment in mouse. Measurement started 6 day after tumor allograft when the size of tumors could be accurately measured. (B) The relative tumor size is defined as the tumor volume on the indicated day divided by that on day 0. For each treatment 8–9 mice were used, and each mouse was transplanted with two tumors on their hind flank. Results shown are from one of the two independent experiments. (C) At the end of the experiment, the Gli1 transcript levels in 5 of randomly sampled tumors were assessed by qPCR. Hh signaling activity was reduced by Mmg RNAi. Data are presented as Mean ± SEM. Statistics: Student's t-Test. **$p < 0.01$, ***$p < 0.001$.

## Materials and Methods

### Plasmids and generation of Myomegalin knockout CRISPR cell clones

Human PDE4D3 is generously provided by Marco Conti lab at UCSF, and was subcloned to include HA and EGFP tag. Myomegalin-C is cloned by RT-PCR with a mouse total mRNA library, and subcloned to included Flag and EGFP tag.

The two gRNA were designed via the Guide Design Resources of Feng Zhang lab at MIT(https://zlab.bio/guide-design-resources). The two gRNAs were cloned into the backbone of pX330-U6-Chimeric_BB-CBh-hSpCas9 (Addgene 42230), and transfected into MEF cells together with EGFP via lipofectamine 2000. 48hr after transfection, EGFP-positive cells were sorted by flow cytometer and plated into individual wells in 96-well plate. Individual cell clones were cultured for 2-4 weeks, and transferred to 24-well plate for further expansion.

### Western blot

Cells were lysed on ice in RIPA buffer containing 25mM Tris-HCl (pH7.6), 150mM Nacl, 1% NP-40, 1% sodium deoxycholate, 0.1% SDS, 1mM PMSF, 10mM sodium fluoride, 2mM sodium pyrophosphate, 1mM sodium orthovanadate, Roche protease inhibitor cocktail and Roche PhosSTOP inhibitor cocktail for 30 min. Lysates were cleared with centrifugation at 13,000 rpm for 30 min at 4℃. Protein concentrations of the supernatants were determined with BCA protein assay kit (Pierce). Protein samples were boiled in 6x SDS sample buffer for 10 min, and resolved in SDS-PAGE. Protein binds were transferred to PVDF membrane (88520, Thermofisher), which were blocked in Tris buffer (PH7.0) containing 0.1% Tween-20 and 5% BSA. The membrane was incubated in primary antibodies (diluted in blocking buffer) overnight at 4 ℃, and washed 3 times before incubation with HRP-conjugated secondary antibodies. Protein bands were visualized with ECL Western Blot substrate (Pierce, 32109).

Primary antibodies used: mouse anti-GAPDH (ab9484, Abcam), rabbit anti-phosphoPKA-T197 (5661S, Cell Siganling), rabbit anti-phosphoCREB-S133 (9198S, Cell Signaling), mouse anti-PKA (610625, BD Biosciences,), rabbit anti-Gli3 (NBP2-16665, NOVOUS), rabbit anti-Gli1 (V812, Cell Signaling), rabbit anti-Myomegalin (PA5-30324, Invitrogen).

### Co-Immunoprecipitation

Plasmids were transfection into HEK293Tcells with lipofectamine 2000 reagent (Invitrogen) according to manufacturer's instruction. Plasmids used : HA-PDE4D3, 3xFlag-Mmg-C560 and 3xFlag-vector (E4026, Sigma, MO). 24hr after transfection, cells were lysed in ELB buffer (150mM NaCl, 1% TritonX100, 50mM Tris pH8.0, 5mM EDTA, 5mM NaF, 2mM $Na_3VO_4$) supplemented with Protease inhibitor cocktail (Roche 11836170001) for 30min at 4˚C. Lysates were cleared by centrifugation at 14,000rpm for 15min. Protein concentration of supernatants were determined using Pierce BCA Protein Assay Kit (Thermo Scientific). Equal amount of protein was loaded to the anti-Flag M2 Magnetic beads (M8823, Sigma) and anti-HA Magnetic beads (88836, Thermo Scientific) and incubated for 1h at room temperature. Beads were washed according to manufacturer's instruction and incubated with 2x Laemmli sample buffer at 95˚C for 5min. Samples were loaded to 10% SDS-PAGE gel and western blot was performed. Antibodies used: HA-tag rabbit antibody (3724S, Cell Signaling), anti-Flag M2 antibody (F1804, Sigma).

### Immunofluorescence staining

NIH3T3 or MEF cells grown on Poly-D-Lysine (A003E, Sigma) coated coverslips were fixed with 4% paraformaldehyde for 10min at room temperature. Cells were then blocked with 2% donkey serum and 0.1% triton in PBS for 1h. Primary and secondary antibodies are incubated with cells in the blocking buffer. Images were taken with LEICA DMi8 microscopy, or Zeiss LSM880

confocal microscope, with 60x oil lens.

Primary antibodies used: anti-Flag M2 antibody (F1804, Sigma), anti-mouse Pericentrin (611814, BD Biosciences), anti-rabbit myomegalin antibody (PA552969, Invitrogen), anti-rabbit GFP antibody (A11122, Thermo Fisher), mouse anti-acetylated tubulin (T6793, SIGMA), goat anti-Gli2 (AF3635, R&D SYSTEMS), rabbit anti-pPKA (ab59218, Abcam).

**Quantification of PhosphoPKA, PDE4D3 and Gli2**

The levels of phosphoPKA and EGFP-PDE4D3 in centrosome were measured using ImageJ software as follows. First, an area of interest (AOI) was delineated based on the signal intensity of pericentrin staining; second, the mean gray value in AOI was measured in the phosphoPKA or EGFP-PD4D3 channel (F1); third, the contour of AOI was manually dragged to a nearby region within the cell, and the mean gray value of the enclosed area was measured as background (F2). The final values of phosphoPKA and PDE4D3 were calculated as F = F1-F2.

To quantify Gli2 levels at the cilium tips, the contour of the cilium tips was outlines in red channel (acetylated tubulin staining). The mean gray density in the enclosed area was measure in green channel (Gli2 staining). The background gray density was measured and subtracted to obtain the final Gli2 intensity at the cilium tips.

For each condition, 35-60 cells were measured. In myomegalin rescue experiment, only cells that were transfected with EGFP-Mmg are measured. Data analysis were done with Graphpad Prism 8.0 Software. Kruskal–Wallis non-parametric One-Way ANOVA was used for statistical analysis.

**Quantitative PCR**

Cells were plated in 6-well plates at 0.5 x $10^6$ cells per well and cultured overnight. For Hh induction, cells were stimulated with 100nM SAG in starvation medium (0.5% FBS in DMEM) for 20-24hr. Total RNAs were isolated with Trizol reagent. The concentration of total RNA was normalized, and the same amount of RNA was mixed with qScript XLT-1 Step, RT-qPCR ToughMix (Quantabio 66149433,) together with specific TaqMan expression assays. The real-time PCR is performed in QuantStudio 3 (ThermoFisher).

The following TaqMan gene expression probes used: Mm00494654_g1 (Gli1), Mm00626240_m1 and Mm01257004_m1 (Mmg), Mm99999915_g1 (GAPDH).

**Primary culture of GNPs and Brdu incorporation assay**

Neonate CD1 mouse were sacrificed at P7. The cerebellum was taken out and cut into small pieces with razor blades, incubated at 37˚C for 15min in digestion buffer (HBSS with 20mM HEPES, PH 7.3, supplemented with trypsin and DNase I). At the end of incubation, digestion buffer was aspirated and replaced with Neurobasal medium with 250U/ml DNase I. Tissues were then triturated with pipet tips and polished Pasteur pipettes. After seated for 2min, dissociated cells were collected from the upper layer and centrifuged at 1000rpm for 5 min. Cells were washed one time, and resuspended in Neurobasal, supplemented with B27 (17504044, Gibco), Glutamax, and 1% Penicillin/streptomycin. Cells were then plated on coverslips coated with Poly-D-Lysine and Laminin. Lentivirus expressing Mmg shRNA were added 5hr after plating, and incubated overnight. 48hr after plating, 10nM SAG was added to the cells and incubated overnight. Brdu (20μM) was added to the culture and pulse labeled for 4hr, after which cells are fixed with 4% paraformaldehyde. Brdu immunostaining were performed with mouse-anti-Brdu antibody (662411Ig, Proteintech).

**Medulloblastoma xenograft mouse model**

All the *in vivo* surgery steps and treatments were performed in accordance with the animal protocols approved by UC Merced's Institutional Biosafety Committee (IACUC). MB56 tumor cells were cultured in neurobasal medium supplemented with B-27 (21103-049, Thermofisher).

Cells were infected with lentiviral particles of shRNA against Myomegalin or control shRNA. 48hr later, cells were then collected, centrifuged and resuspended in PBS at 2 x $10^7$cells per 50ul. 50ul cells were mixed with Matrigel (354234, ThermoFisher) at 1:1 volume ration. The 100ul mixture was slowly injected into hind flanks of 8-10 nude mice of 7-week old (002019, Jackson Laboratory) under isoflurane anesthesia. 6-days after injection, the tumor volume was measured daily with digital caliper for two weeks. At the end of the experiments, mice were euthanized and 5-6 tumors were harvested randomly. Tumor tissues were proceeded to RNA extraction and qPCR. To generate a tumor growth curve, the relative tumor size is calculated as the ration of tumor size on each day over the size of the same tumor on day 1 of measurement.

**Quantification and Statistical Analysis**

All statistical analysis was performed using Graphpad Prism 8.0 Software (Graphpad Software; La Jolla, CA, USA). Statistical significance was determined by Student's t-Test or Kruskal–Wallis non-parametric One-Way ANOVA as mentioned in the figure legends.

## Acknowledgements

We thank Dr. Marco Conti for their generous gifts of PDE4D constructs, and helpful discussions. We thank Sammy Villa for cloning the CRISPR construct and the initial transfection of MEF cells. We thank Lavpreet Jammu, Anh Diep and Christi Waer for initial characterization of Myomegalin shRNA and for generating Myomegalin and PDE4D3 constructs. We thank Dr. Lin Gan for helpful discussions on the manuscript. The research was supported by N.I.H. grant R15 CA235749 to X.G.

## Competing Interests

The authors have no competing interests to declare.

## Author contributions

Xuecai Ge: Conception and design of all experiments, Acquisition of a portion of data, Analysis and interpretation of data, Drafting the article
Jingyi Zhang: Acquisition, analysis and interpretation of data on Mmg-PDE4D interaction and GNP culture
Hualing Peng: Acquisition, analysis and interpretation of data on characterization of Mmg CRISPR Knockout clones and mouse tumor model
Winston Ma: Establishment, expanding, initial selection and maintenance of Mmg CRISPR Knockout clones
Amanda Ya: Initial selection and maintenance of Mmg CRISPR Knockout clones, Characterization of INDEL mutations in Mmg CRISPR clones

## References

1 Briscoe J, Therond PP. The mechanisms of Hedgehog signalling and its rolesin developement and disease. *Nat Rev Molecuar Cell Biol* 2013; **14**: 416.

2 Wechsler-Reya RJ, Scott MP. Control of neuronal precursor proliferation in the cerebellum by sonic hedgehog. *Neuron* 1999; **22**: 103–14.

3 Wallace VA. Purkinje-cell-derived Sonic hedgehog regulates granule neuron precursor cell proliferation in the developing mouse cerebellum. *Curr Biol* 1999; **9**: 445–8.

4 Dahmane N, Ruiz i Altaba a. Sonic hedgehog regulates the growth and patterning of the cerebellum. *Development* 1999; **126**: 3089–100.

5 Goodrich L V., Milenković L, Higgins KM, Scott MP. Altered neural cell fates and

medulloblastoma in mouse patched mutants. *Science (80- )* 1997. DOI:10.1126/science.277.5329.1109.

6 Hui C, Angers S. Gli Proteins in Development and Disease. *Annu Rev Cell Dev Biol* 2011; **27**: 513–37.

7 Han Y-G, Alvarez-Buylla A. Role of Primary Cilia in Brain Development and Cancer. *Curr Opin Neuroviology* 2010; **20**: 58–67.

8 Wang B, Li Y. Evidence for the direct involvement of βTrCP in Gli3 protein processing. *Proc Natl Acad Sci U S A* 2006; **103**: 33–8.

9 Tuson M, He M, Anderson K V. Protein kinase A acts at the basal body of the primary cilium to prevent Gli2 activation and ventralization of the mouse neural tube. *Development* 2011; **138**: 4921–30.

10 Epstein DJ, Marti E, Scott MP, McMahon AP. Antagonizing cAMP-dependent protein kinase A in the dorsal CNS activates a conserved Sonic hedgehog signaling pathway. *Development* 1996; **122**: 2885–94.

11 Huang Y, Roelink H, McKnight GS. Protein kinase A deficiency causes axially localized neural tube defects in mice. *J Biol Chem* 2002; **277**: 19889–96.

12 Yamanaka H, Takaharu O, Uehara S, Fukuzawa M. Forskolin, a Hedgehog signal inhibitor, inhibits cell proliferation and induces apoptosis in pediatric tumor cell lines. *Mol Med Rep* 2010. DOI:10.3892/mmr-00000230.

13 Yamanaka H, Oue T, Uehara S, Fukuzawa M. Hedgehog signal inhibitor forskolin suppresses cell proliferation and tumor growth of human rhabdomyosarcoma xenograft. *J Pediatr Surg* 2011. DOI:10.1016/j.jpedsurg.2010.11.010.

14 Tyler Hillman R, Feng BY, Ni J, *et al.* Neuropilins are positive regulators of Hedgehog signal transduction. *Genes Dev* 2011. DOI:10.1101/gad.173054.111.

15 Ge X, Milenkovic L, Suyama K, *et al.* Phosphodiesterase 4D acts downstream of Neuropilin to control Hedgehog signal transduction and the growth of medulloblastoma. *Elife* 2015; **4**.

16 Williams CH, Hempel JE, Hao J, *et al.* An In Vivo Chemical Genetic Screen Identifies Phosphodiesterase 4 as a Pharmacological Target for Hedgehog Signaling Inhibition. *Cell Rep* 2015; **11**: 43–50.

17 Houslay MD. Underpinning compartmentalised cAMP signalling through targeted cAMP breakdown. Trends Biochem. Sci. 2010; **35**: 91–100.

18 McCormick K, Baillie GS. Compartmentalisation of second messenger signalling pathways. *Curr Opin Genet Dev* 2014; **27**: 20–5.

19 Zaccolo M, Pozzan T. Discrete microdomains with high concentration of cAMP in stimulated rat neonatal cardiac myocytes. *Science (80- )* 2002; **295**: 1711–5.

20 Barzi M, Berenguer J, Menendez A, Alvarez-Rodriguez R, Pons S. Sonic-hedgehog-mediated proliferation requires the localization of PKA to the cilium base. *J Cell Sci* 2010; **123**: 62–9.

21 Verde I, Pahlke G, Salanova M, *et al.* Myomegalin is a Novel Protein of the Golgi/Centrosome That Interacts with a Cyclic Nucleotide Phosphodiesterase. *J Biol Chem* 2001; **276**: 11189–98.

22 Roubin R, Acquaviva C, Chevrier V, *et al.* Myomegalin is necessary for the formation of

centrosomal and Golgi-derived microtubules. *Biol Open* 2013; **2**: 238–50.

23 Shaywitz AJ, Greenberg ME. CREB: A Stimulus-Induced Transcription Factor Activated by A Diverse Array of Extracellular Signals. *Annu Rev Biochem* 1999. DOI:10.1146/annurev.biochem.68.1.821.

24 Humke EW, Dorn K V., Milenkovic L, Scott MP, Rohatgi R. The output of Hedgehog signaling is controlled by the dynamic association between Suppressor of Fused and the Gli proteins. *Genes Dev* 2010. DOI:10.1101/gad.1902910.

25 Tukachinsky H, Lopez L V., Salic A. A mechanism for vertebrate Hedgehog signaling: Recruitment to cilia and dissociation of SuFu-Gli protein complexes. *J Cell Biol* 2010. DOI:10.1083/jcb.201004108.

26 Kool M, Korshunov A, Remke M, *et al.* Molecular subgroups of medulloblastoma: An international meta-analysis of transcriptome, genetic aberrations, and clinical data of WNT, SHH, Group 3, and Group 4 medulloblastomas. *Acta Neuropathol* 2012; **123**: 473–84.

27 Richter W, Jin S-LC, Conti M. Splice variants of the cyclic nucleotide phosphodiesterase PDE4D are differentially expressed and regulated in rat tissue. *Biochem J* 2005; **388**: 803–11.

28 Purzner T, Purzner J, Buckstaff T, *et al.* Developmental phosphoproteomics identifies the kinase CK2 as a driver of Hedgehog signaling and a therapeutic target in medulloblastoma. *Sci Signal* 2018. DOI:10.1126/scisignal.aau5147.

29 Ogden SK, Fei DL, Schilling NS, Ahmed YF, Hwa J, Robbins DJ. G protein Gαi functions immediately downstream of Smoothened in Hedgehog signalling. *Nature* 2008. DOI:10.1038/nature07459.

30 Mukhopadhyay S, Wen X, Ratti N, *et al.* The ciliary G-protein-coupled receptor Gpr161 negatively regulates the sonic hedgehog pathway via cAMP signaling. *Cell* 2013; **152**: 210–23.

31 Ge X, Milenkovic L, Suyama K, *et al.* Phosphodiesterase 4D acts downstream of Neuropilin to control Hedgehog signal transduction and the growth of medulloblastoma. *Elife* 2015; **4**. DOI:10.7554/eLife.07068.

32 Maurice DH, Ke H, Ahmad F, Wang Y, Chung J, Manganiello VC. Advances in targeting cyclic nucleotide phosphodiesterases. *Nat Rev Drug Discov* 2014; **13**: 290–314.

33 Yauch RL, Dijkgraaf GJP, Alicke B, *et al.* Smoothened mutation confers resistance to a Hedgehog pathway inhibitor in medulloblastoma. *Science* 2009; **326**: 572–4.

34 Gavaldà A, Roberts RS. Phosphodiesterase-4 inhibitors: a review of current developments (2010 - 2012). *Expert Opin Ther Pat* 2013; **23**: 997–1016.